Electronic Supplementary Material (ESI) for Journal of Materials Chemistry A.
This journal is © The Royal Society of Chemistry 2018

Supporting Information

Oxygen Vacancy-originated Highly Active Electrocatalysts for Oxygen Evolution Reaction

Shigeto Hirai*, Kazuki Morita, Kenji Yasuoka, Taizo Shibuya, Yujiro Tojo, Yoichi Kamihara, Akira Miura, Hisao Suzuki, Tomoya Ohno, Takeshi Matsuda, and Shunsuke Yagi

I. Experimental

Further details of computational methods

DFT calculations were conducted with a well converged plane-wave cutoff of 500 eV and the Brillouin-zone sampled by a 4×4×2 Monkhorst-Pack mesh[S1]. For δ=0.25, there are 2 non-equivalent configurations out of ${}_{12}C_1 = 12$ configurations. For δ=0.5 and 0.75, 11 and 25 O* configurations out of 66 and 220 configurations were calculated, respectively.

For the density of states (DOS), ionic positions were optimized by minimizing the Hellmann-Feynman force[S2,S3]. Averaged DOS were calculated for δ = 0, 0.25, 0.50, 0.75. Only configurations that converged to the known stable magnetic structure[33], checkerboard anti-ferromagnetic order for V and stripe anti-ferromagnetic order for Fe, were included in the average. Note that the total energy of the excluded configurations are high; the statistical average is not significantly affected even if they are considered. The averaged DOS $\langle n(e)\rangle$ were calculated by the following equation:

$$\langle n(e)\rangle = \frac{\sum_i w_i n_i(e)\, e^{\frac{E_i}{k_B T}}}{\sum_i e^{\frac{E_i}{k_B T}}}$$

where w_i is the statistical weight, E_i is the total energy of i-th configuration, k_B is the Boltzmann constant, T is the temperature. The temperature T was set to 300 K reflecting the temperature of the electrochemical measurements. It should be noted that the choice of the temperature had little effect on the results.

Average O*-O* distances of the nearest neighbors $\langle r^{min}(\delta=x)\rangle$ were calculated for δ =0.17, 0.25, 0.33, 0.42, 0.5, 0.58, 0.67, 0.75. The system was described by combinations of three supercells, each of which being considered as a local system

representing δ_{local}=0, 0.25, 0.50, 0.75. The ionic positions were fixed at the bulk positions. For example, δ=0.5 is expressed in three ways: (δ_{local}=0.0)+ (δ_{local}=0.75)+ (δ_{local}=0.75), (δ_{local}=0.25)+ (δ_{local}=0.5)+ (δ_{local}=0.75), (δ_{local}=0.5)+ (δ_{local}=0.5)+ (δ_{local}=0.5). This procedure can be described by the following equations:

$$\langle r^{\min}(\delta=x)\rangle=\frac{\sum_I w_I r_I^{\min}(\delta=x)\, e^{\frac{E_I(\delta=x)}{k_B T}}}{\sum_I e^{\frac{E_I(\delta=x)}{k_B T}}}$$

where

$$E_I(\delta=x)=E_{\mathrm{local}\,A}+E_{\mathrm{local}\,B}+E_{\mathrm{local}\,C}$$
$$w_I(\delta=x)=w_{\mathrm{local}\,A}\, w_{\mathrm{local}\,B}\, w_{\mathrm{local}\,C}$$
$$r_I^{\min}(\delta=x)=\min(r_{\mathrm{local}\,A}^{\min}, r_{\mathrm{local}\,B}^{\min}, r_{\mathrm{local}\,C}^{\min})$$

A, *B* and *C* is a supercell with oxygen vacancies of δ=0.00, 0.25, 0.50 or 0.75, which were exhaustively chosen to satisfy the following relationship:

$$x=(\delta_{\mathrm{local}\,A}+\delta_{\mathrm{local}\,B}+\delta_{\mathrm{local}\,C})/3$$

Here, w_I and $E_I(\delta=x)$ is the total energy of *I*-th structure with the oxygen vacancy of *x*. The temperature *T* was set to 1573 K accounting the temperature of the preparation process. Similar to the case with the DOS, the choice of the temperature had little effect on the results.

II. Supplementary Results

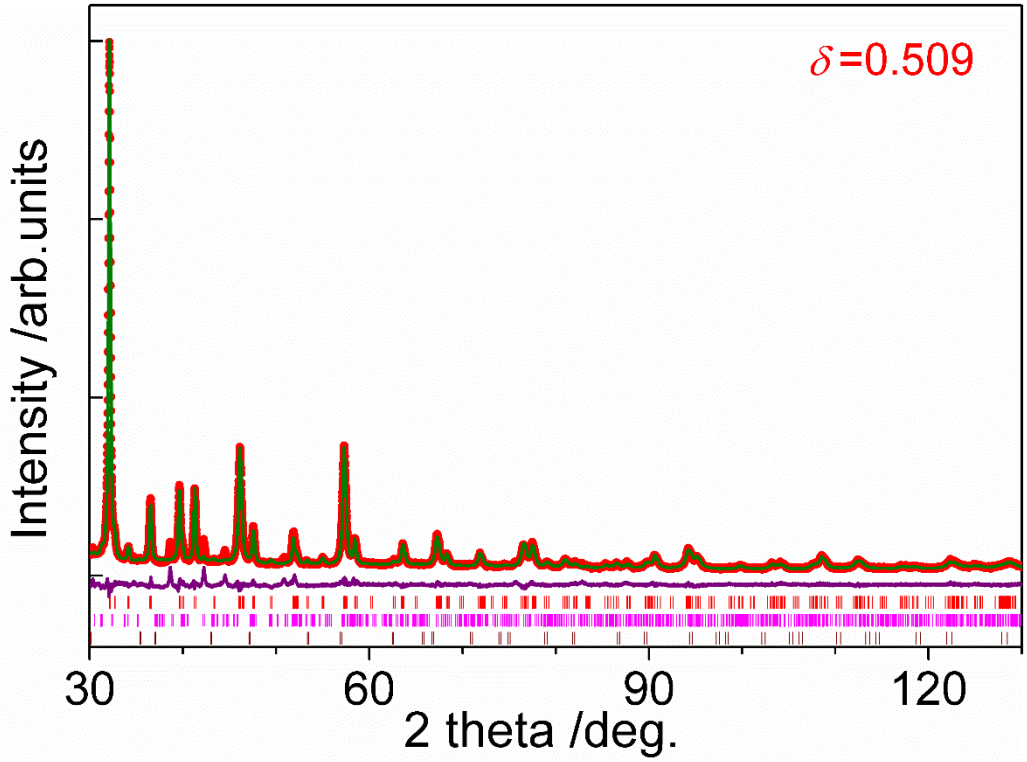

Fig. S1. XRD and the Rietveld refinement of $Sr_2VFeAsO_{3-\delta}$. Here, we show the representative XRD profile and Rietveld refinement result for $Sr_2VFeAsO_{3-\delta}$(δ = 0.509). The red circles and the green line indicate the observed and calculated profile, respectively. The purple line displays the difference between the observed and calculated profile. The red tick marks indicate the Bragg reflection positions of $Sr_2VFeAsO_{3-\delta}$. The pink and brown tick marks indicate the Bragg reflection positions of the minor secondary phase, SrV_2O_6 and Fe_3O_4, respectively. Wavelength λ = 0.15406 nm. The samples used for the characterization and electrochemical measurements in this study are the same samples used for characterization in Tojo *et al.*[17]. Therefore, this figure was reproduced from Tojo *et al.*[17]. Further details and the XRD profiles for δ= 0.078, 0.237, and 0.631 are shown in Tojo *et al.*[17].

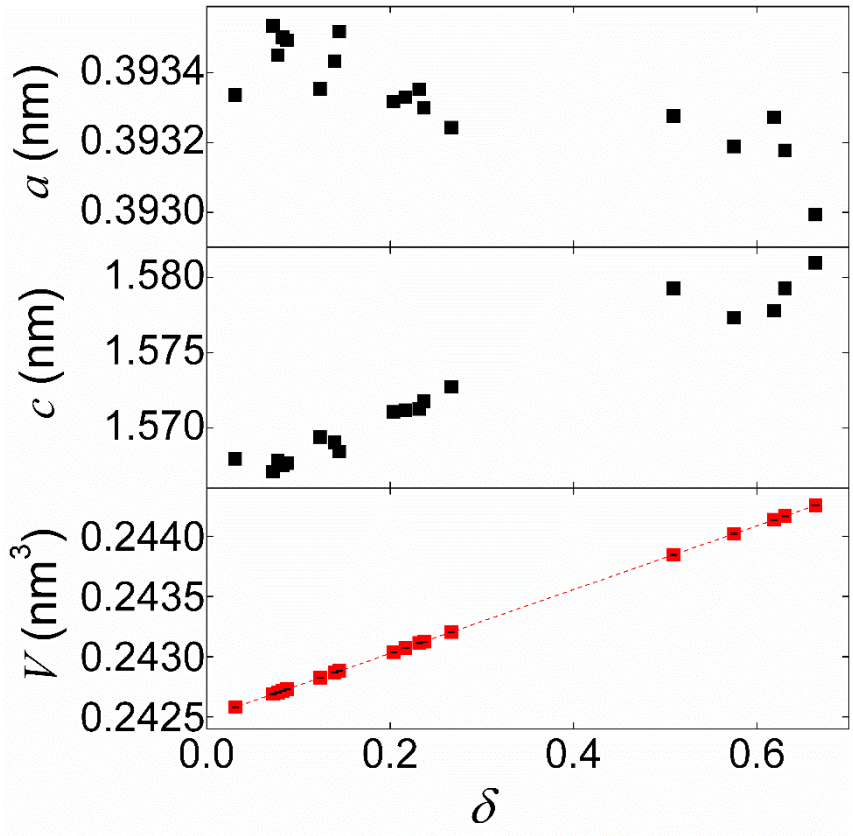

Fig. S2. Evolution of the tetragonal lattice parameter *a*, *c*, unit cell volume (*V*) for $Sr_2VFeAsO_{3-\delta}$. Standard deviation for the data is within the symbol size. The oxygen vacancy δ was determined by the linear correlation of $\delta = 377.349V(\mathrm{nm}^{-3})-91.5057$. The samples used for the characterization in this study are the same samples used for characterization in Tojo *et al.*[17]. Therefore, this figure was reproduced from Tojo *et al.*[17].

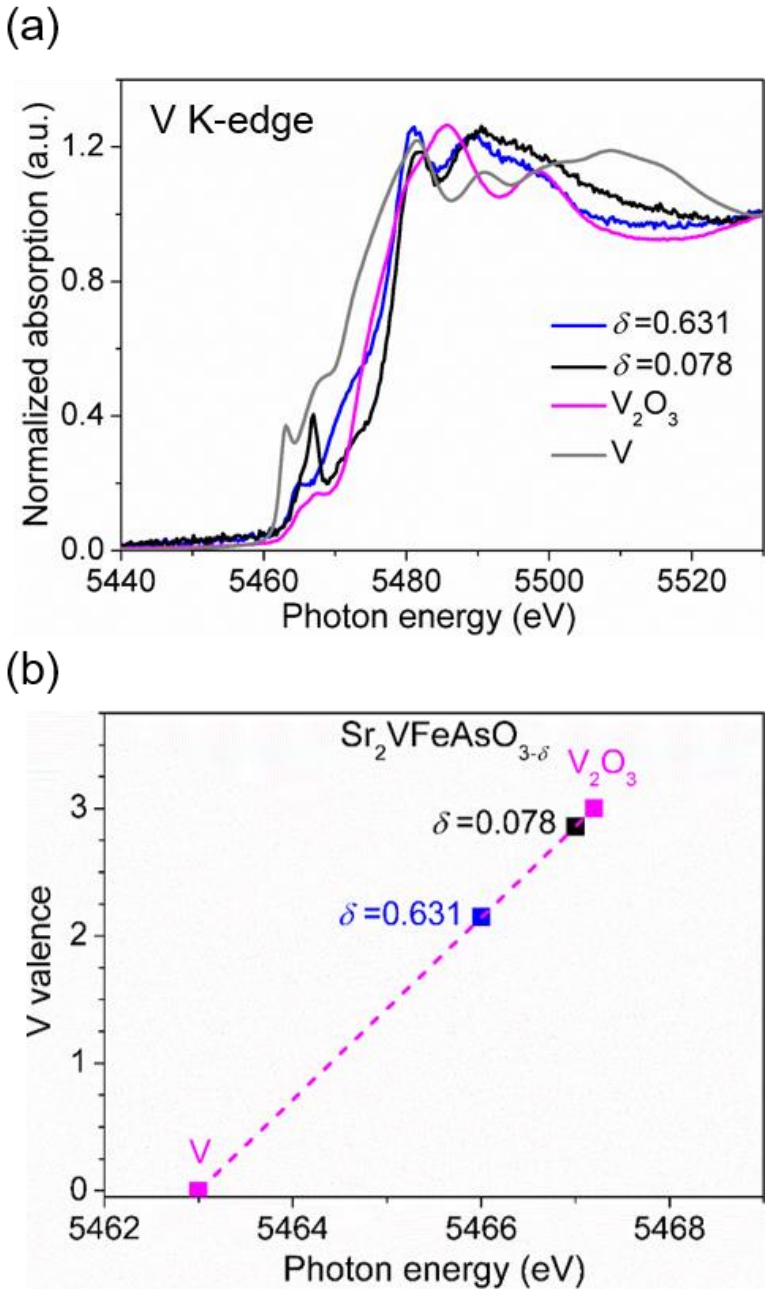

Fig. S3. V K-edge X-ray absorption near-edge structure (XANES) spectra for $Sr_2VFeAsO_{3-\delta}$. (a) Normalized V K-edge XANES spectra for δ=0.078 and 0.631. V and V_2O_3 were used as standard materials. (b) V valence of $Sr_2VFeAsO_{3-\delta}$(δ =0.078 and 0.631), V and V_2O_3 as a function of the photon energy for the V pre-edge peak. The dashed line is a guide for the eyes. This figure is consistent with the V valence obtained by the XRF V-$K_{\alpha 1}$ in Tojo *et al.*[17] and confirms that the V valence in this study is between 2 and 3. Here, the pre-edge peak characteristic for V was chosen as a reference since the absorption edge shows a very small energy shift in the case of V [S4].

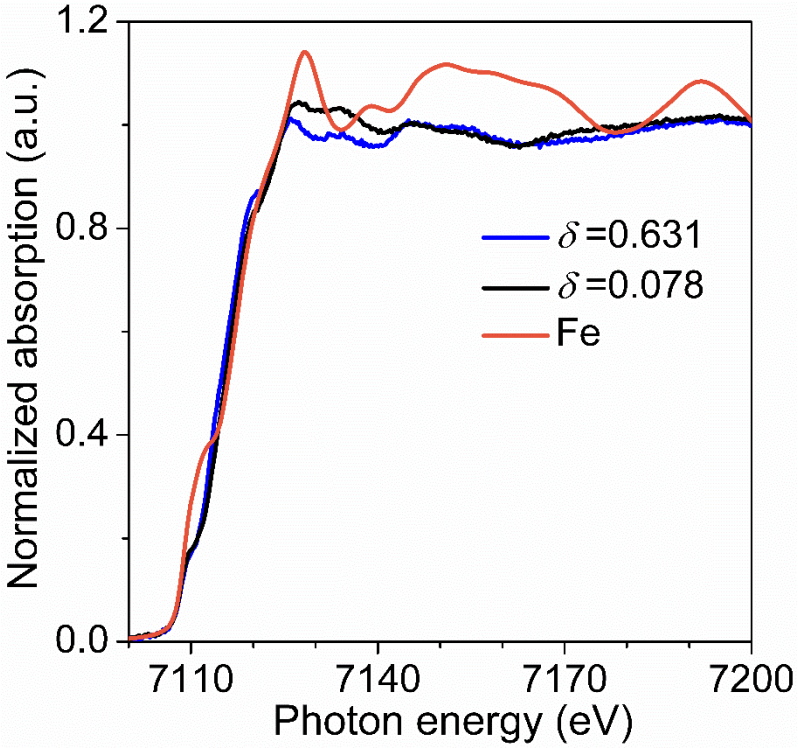

Fig. S4. Fe K-edge XANES spectra for $Sr_2VFeAsO_{3-\delta}$. Normalized Fe K-edge XANES spectra for δ=0.078 and 0.631. Fe was used as a standard material. The Fe absorption edge of δ=0.631 does not show any energy shift with respect to δ=0.078. Therefore, the valence of Fe remains zero throughout the system. This result is also consistent with the unshifted XRF Fe-K$_\alpha$ in Tojo *et al.*[17].

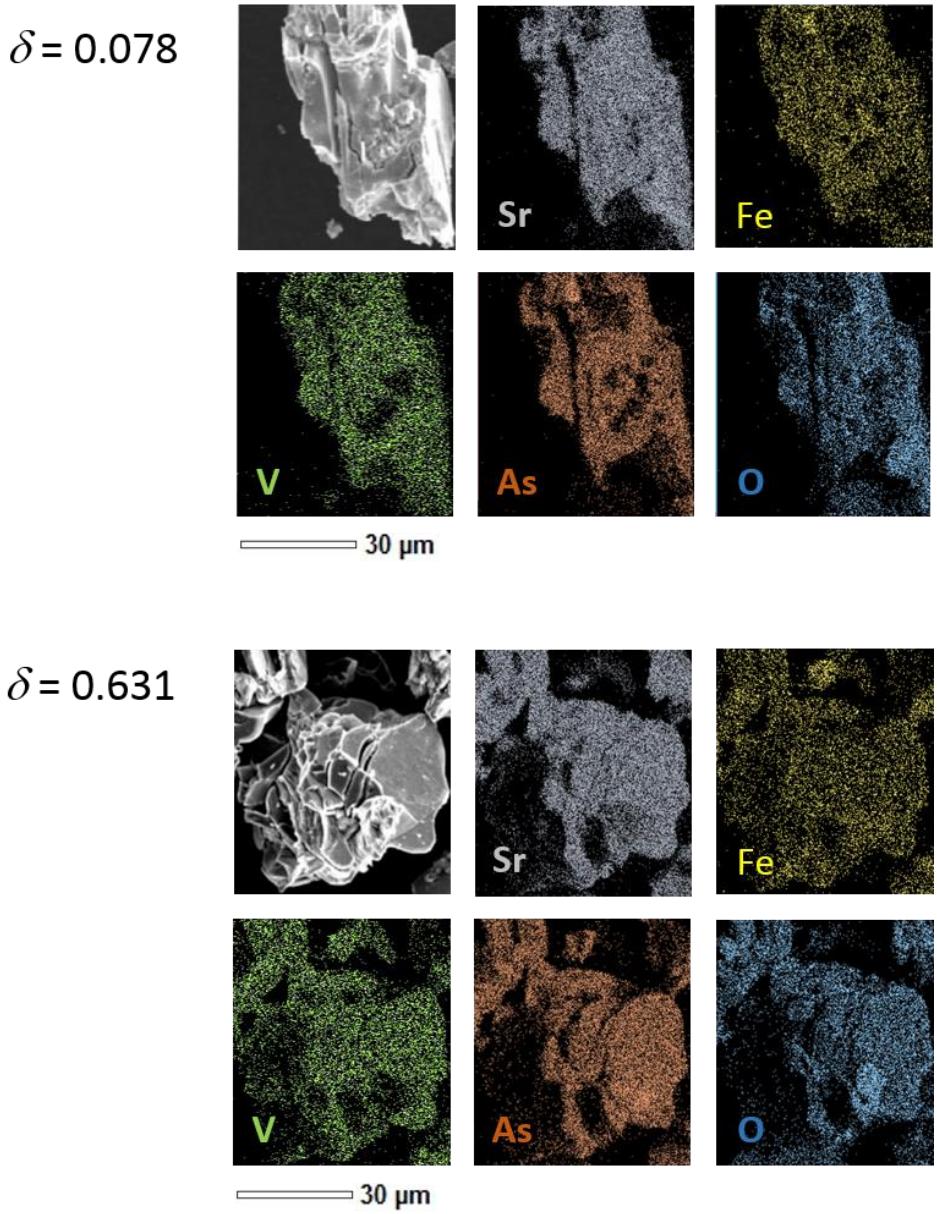

Fig. S5. SEM images of $Sr_2VFeAsO_{3-\delta}$. The representative SEM images and the EDX elemental mapping of $Sr_2VFeAsO_{3-\delta}$ (δ = 0.078 and 0.631).

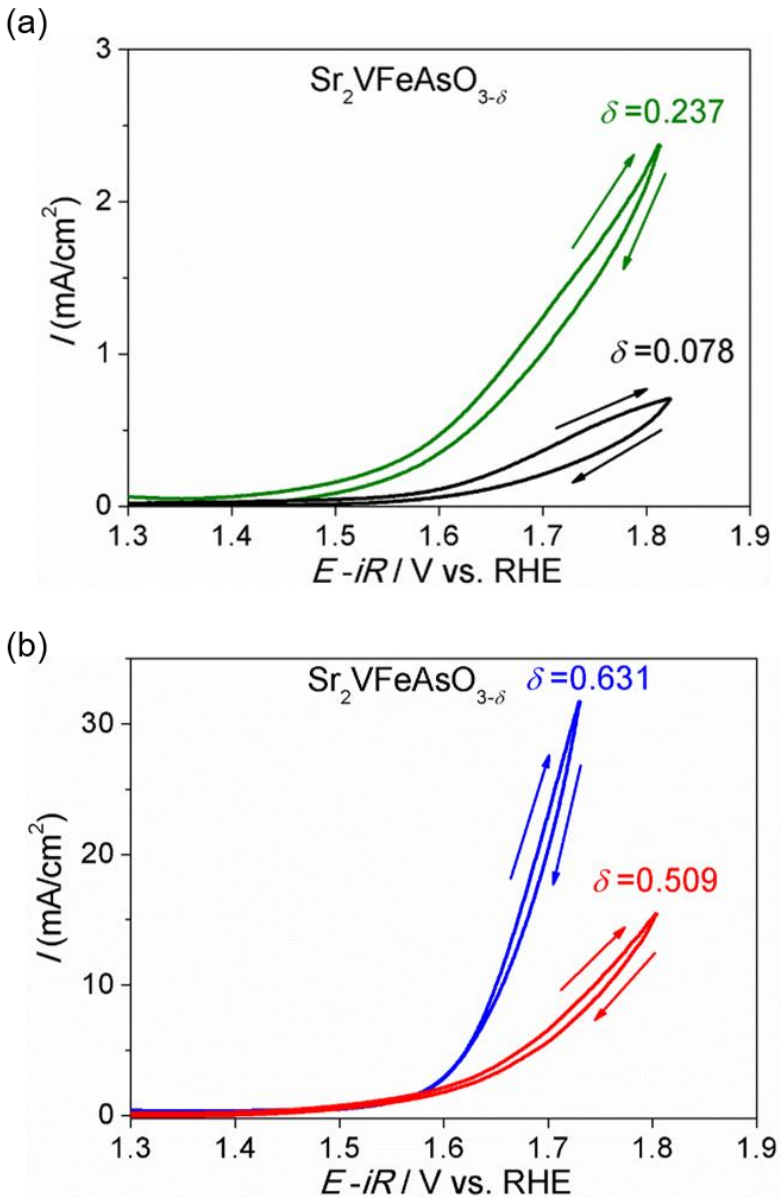

Fig. S6. The OER catalytic activity of $Sr_2VFeAsO_{3-\delta}$. (a, b) The cyclic voltammograms for $Sr_2VFeAsO_{3-\delta}$ (δ = 0.078, 0.237, 0.509, 0.631).

(a)

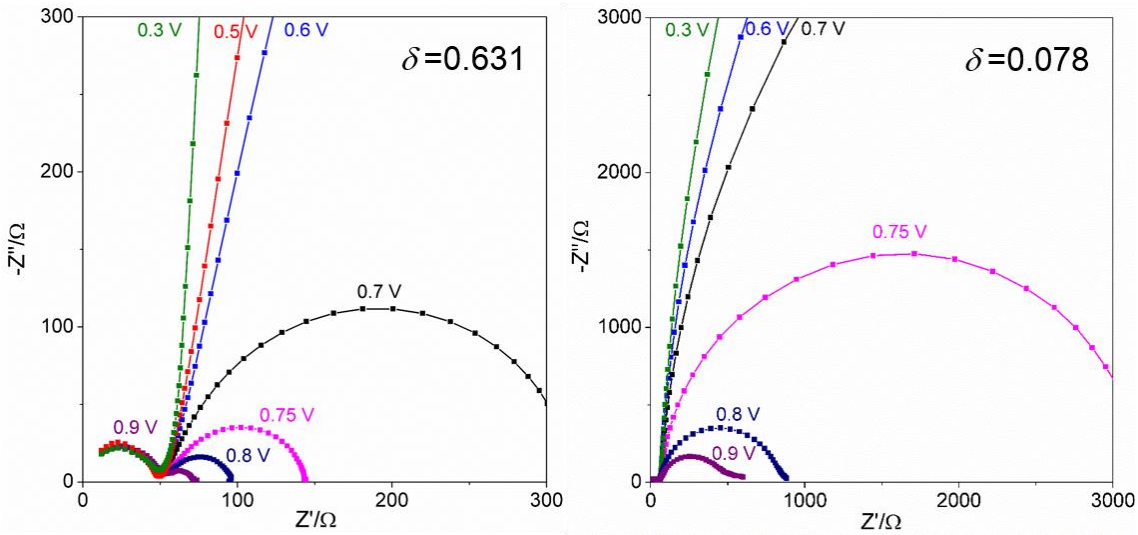

(b)

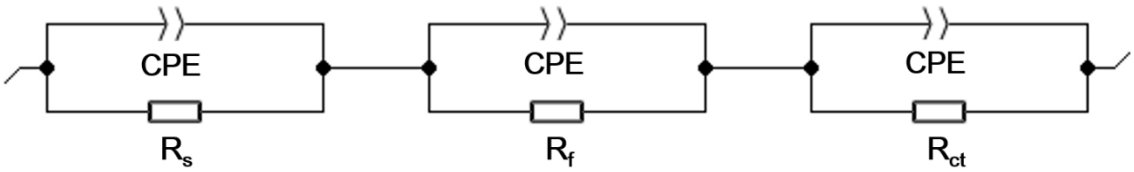

Fig. S7. The electrochemical impedance spectra of $Sr_2VFeAsO_{3-\delta}$. (a) Nyquist plots for $Sr_2VFeAsO_{3-\delta}$ (δ = 0.078 and 0.631) at 0.3-0.9 V vs. Hg/HgO (1.226-1.826 V vs. RHE). Since the oxygen evolution reaction proceeds above 0.5 V vs. Hg/HgO (1.426 vs. RHE) for δ = 0.631, the impedance shows a dramatic decrease due to the charge transfer resistance contribution from the oxygen evolution reaction. (b) The equivalent circuit used for fitting the electrochemical impedance spectra (EIS) of $Sr_2VFeAsO_{3-\delta}$(δ = 0.078 and 0.631). R_s, R_f and R_{ct} denote the solution resistance, the film resistance and the charge transfer resistance, respectively.

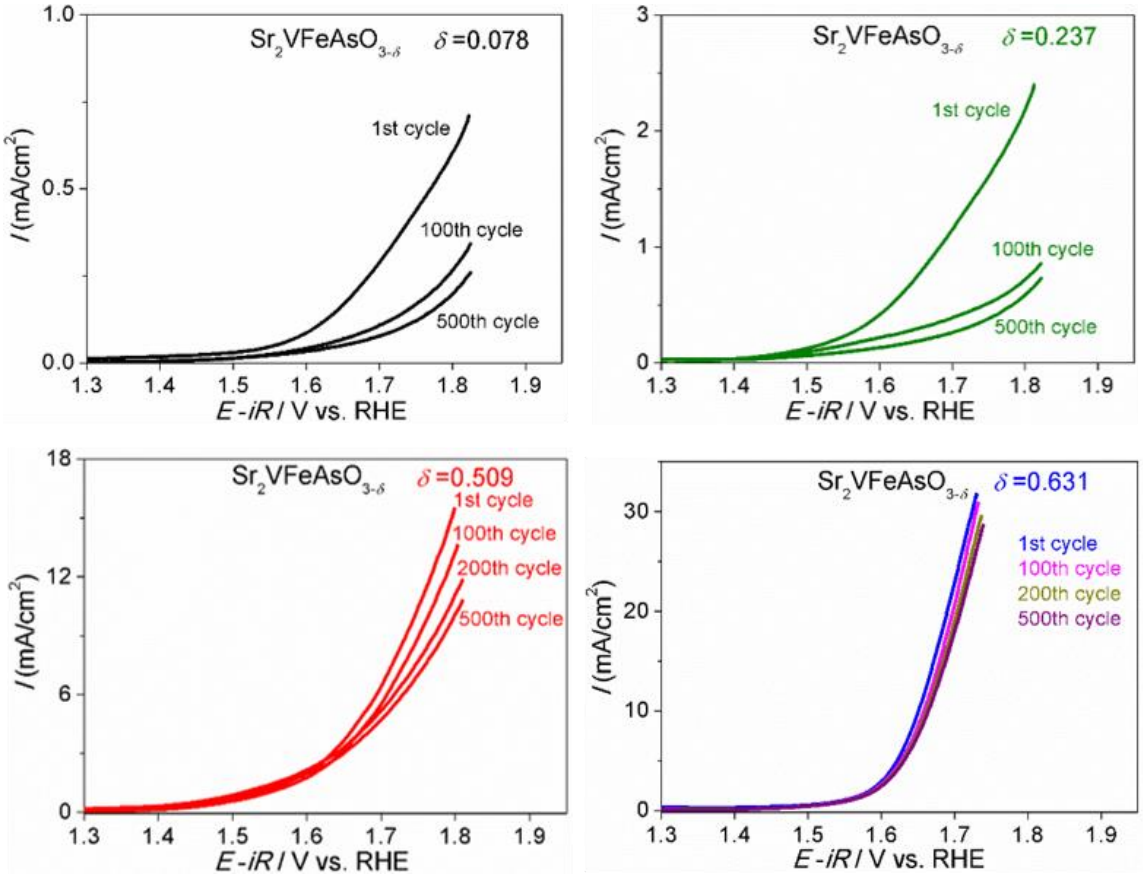

Fig. S8. The OER catalytic stability of $Sr_2VFeAsO_{3-\delta}$. The cycle dependence of the linear sweep voltammograms for $Sr_2VFeAsO_{3-\delta}$ (δ = 0.078, 0.237, 0.509, 0.631). The OER measurements were conducted at the scan rate of 10 mV/s in 0.1 M KOH solution. The OER activity for δ>0.5 retains 75 % of the initial value up to 100-500 cycles, while that for δ>0.5 becomes less than half within 100 cycles.

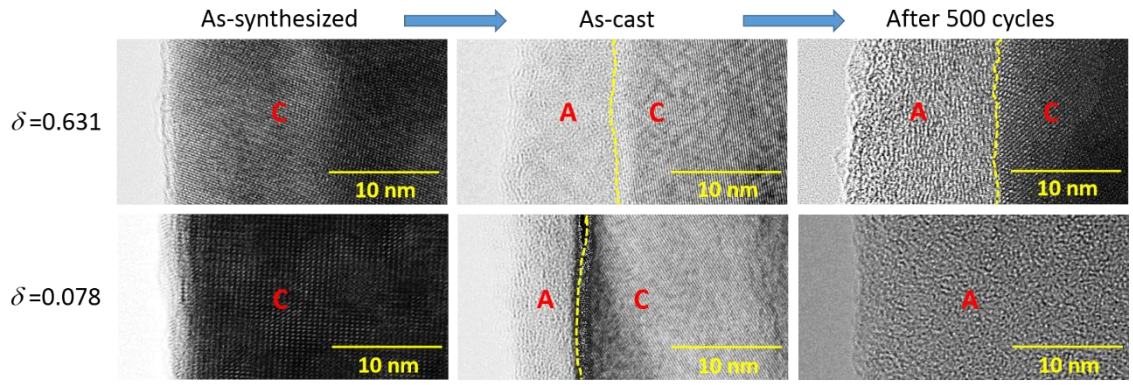

Fig. S9. The OER catalytic stability of $Sr_2VFeAsO_{3-\delta}$. HRTEM images of as-synthesized, as-cast and after 500 OER cycles for δ = 0.078 and 0.631 are shown. The boundaries between the crystalline region (C) and the amorphous region (A) are divided by yellow dotted lines. The robust crystalline layer is retained beneath the amorphous layer for δ = 0.631 even after 500 OER cycles.

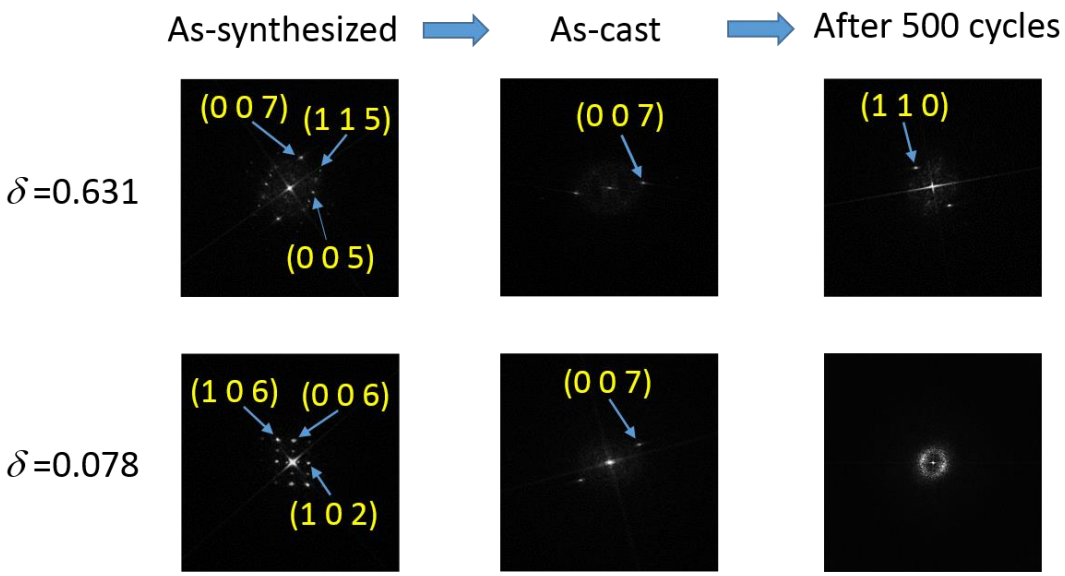

Fig. S10. Fast Fourier transform (FFT) images of $Sr_2VFeAsO_{3-\delta}$. FFT images of as-synthesized, as-cast and after 500 OER cycles for δ = 0.078 and 0.631 are shown. All the FFT images were obtained from the 10-20 nm surface regions of 10 x 10 nm^2.

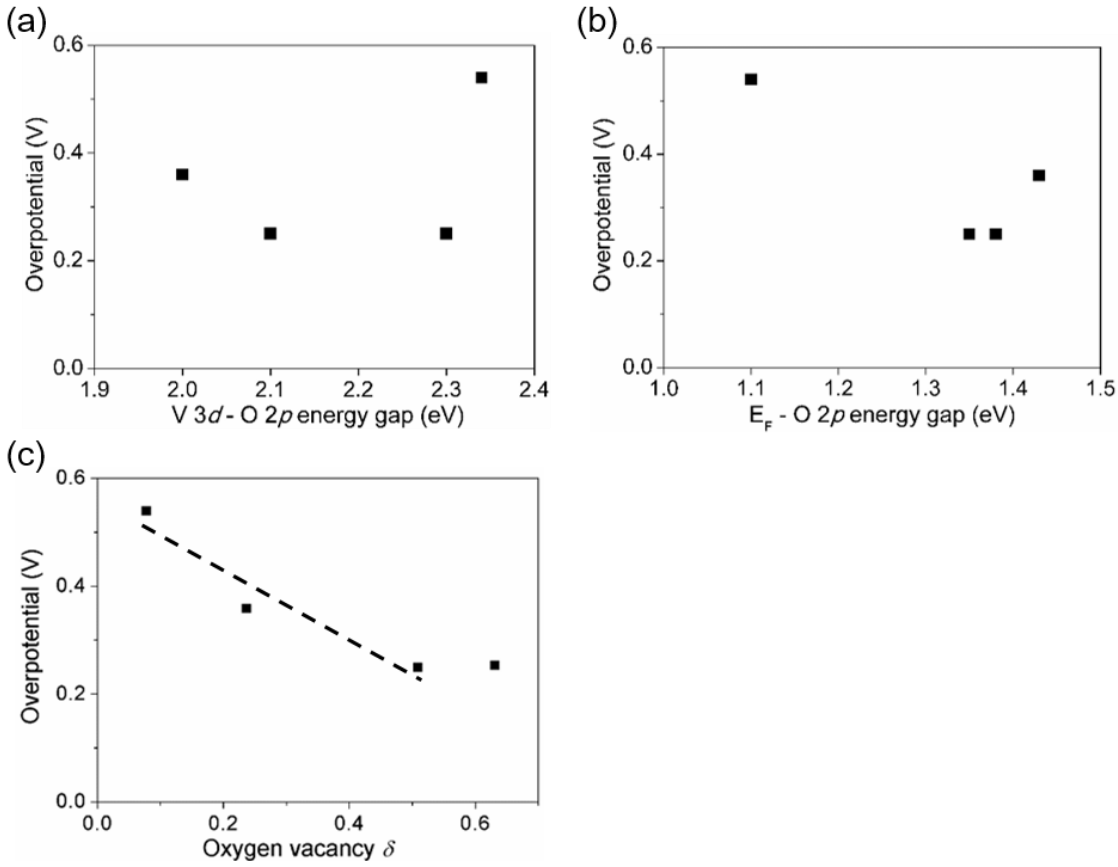

Fig. S11. Overpotential of $Sr_2VFeAsO_{3-\delta}$. (a) The relationship between V 3*d*- O 2*p* energy gap and the overpotential of $Sr_2VFeAsO_{3-\delta}$ (δ=0, 0.25, 0.50, 0.75). (b) The relationship between E_F- O 2*p* energy gap and the overpotential of $Sr_2VFeAsO_{3-\delta}$ (δ=0, 0.25, 0.50, 0.75). (c) The relationship between the oxygen vacancies and the overpotential of $Sr_2VFeAsO_{3-\delta}$ (δ = 0.078, 0.237, 0.509, 0.631). The dashed line is a guide for the eyes.

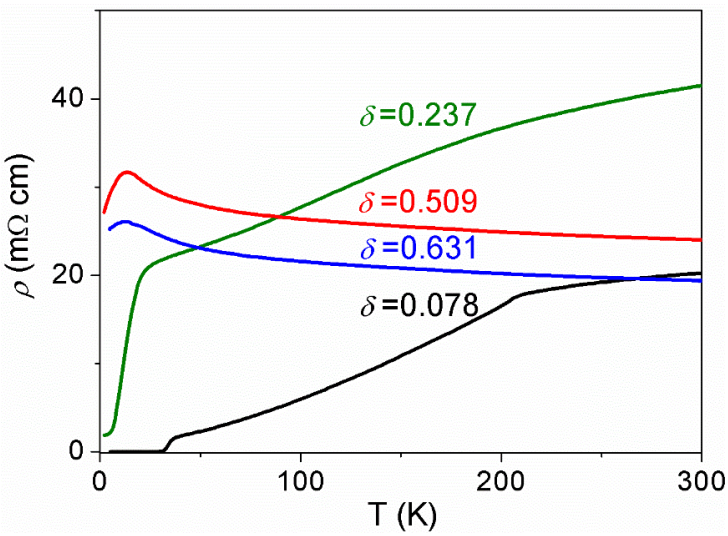

Fig. S12. Electrical transport information of $Sr_2VFeAsO_{3-\delta}$. Temperature dependence of the electrical resistivity for $Sr_2VFeAsO_{3-\delta}$ (δ = 0.078, 0.237, 0.509, 0.631). The samples used for the characterization in this study are the same samples used for characterization in Tojo *et al.*[17]. Therefore, this figure was reproduced from Tojo *et al.*[17].

Table S1. Crystallographic results for $Sr_2VFeAsO_{3-\delta}$. These results were obtained by conducting Rietveld refinement on the XRD profile of $\delta = 0.509$. All these samples adopt the space group of *P*4/*nmm*. Atomic positions are Sr1 (0.75, 0.75, *z*), Sr2 (0.75, 0.75, *z*), V (0.25, 0.25, *z*), Fe (0.25, 0.75, 0), As (0.25, 0.25, *z*), O1 (0.25, 0.75, *z*) and O2 (0.25, 0.25, *z*). BVS denotes the bond valence sum[S5] obtained by using the V-O bond distance[17]. This table was reproduced from Tojo *et al.*[17].

a (nm)	0.393188(2)
c (nm)	1.57730(1)
V (nm^3)	0.243845(4)
Sr1: *z*	0.1914(1)
Sr2: *z*	0.4128(1)
V: *z*	0.31077(0)
Fe: *z*	0
As: *z*	0.0931(1)
O1: *z*	0.2966(5)
O2: *z*	0.4407(7)
BVS for V	2.81

Table S2. The resistance elements of the equivalent circuit for $Sr_2VFeAsO_{3-\delta}$. These results were obtained by fitting the EIS spectra of (a) $\delta = 0.631$ and (b) $\delta = 0.078$ with the equivalent circuit in Fig. S7. R_s, R_f and R_{ct} denote the solution resistance, the film resistance and the charge transfer resistance, respectively.

(a) $\delta = 0.631$

E vs. Hg/HgO (V)	R_s (Ω)	R_f (Ω)	R_{ct} (Ω)
0.5	50	75000	360(10)
0.6	50	32000	78(2)
0.65	45	2100	46(1)
0.7	45	240	25(1)
0.75	45	75(1)	25(1)
0.8	45	28(1)	24(1)
0.85	44	12(1)	23(2)
0.9	43	8.4(1)	21(2)

(b) $\delta = 0.078$

E vs. Hg/HgO (V)	R_s (Ω)	R_f (Ω)	R_{ct} (Ω)
0.7	50	14000	3100
0.75	45	2900	470(10)
0.8	45	670	200
0.9	44	280	330

Supplementary References

[S1] H. J. Monkhorst and J. D. Pack, *Phys. Rev. B*, 1976, **13**, 5188.

[S2] R. P. Feynman, *Phys. Rev.*, 1939, **56**, 340.

[S3] R. S. Sorbello and B. B. Dasgupta, *Phys. Rev. B*, 1980, **21**, 2196.

[S4] P. Chaurand, J. Rose, V. Briois, M. Salome, O. Proux, V. Nassif, L. Olivi, J. Susini, J.-L. Hazemann and J.-Y. Bottero, *J. Phys. Chem. B*, 2007, **111**, 5101.

[S5] I. D. Brown, *The Chemical Bond in Inorganic Chemistry*, Oxford University Press, Oxford, UK **2002**.